Eur. Phys. J. A **11**, 25–38 (2001)

THE EUROPEAN PHYSICAL JOURNAL A

High-spin spectroscopy of $^{63}_{31}Ga_{32}$ and $^{65}_{31}Ga_{34}$

M. Weiszflog[1,a], G. de Angelis[2], A. Axelsson[3,b], D. Bazzacco[4], F. Becker[5], M. De Poli[2], J. Eberth[5], C. Fahlander[2,6], A. Gadea[2], S. Lunardi[4], D.R. Napoli[2], J. Nyberg[1], C. Rossi Alvarez[4], B. Rubio[7], D. Rudolph[6], S. Skoda[5], H.G. Thomas[5], and R. Wyss[8]

[1] Department of Neutron Research, Uppsala University, 75121 Uppsala, Sweden
[2] INFN, Laboratori Nazionali di Legnaro, 35020 Legnaro, Italy
[3] Department of Radiation Sciences, Uppsala University, 75121 Uppsala, Sweden
[4] Dipartimento di Fisica dell'Università and INFN, 35131 Padova, Italy
[5] Institut für Kernphysik, Universität zu Köln, 50937 Köln, Germany
[6] Lund University, 22100 Lund, Sweden
[7] Instituto de Física Corpuscular, Valencia, Spain
[8] The Royal Institute of Technology, 10044 Stockholm, Sweden

Received: 20 December 2000 / Revised version: 9 April 2001
Communicated by D. Guerreau

Abstract. High-spin states in the nuclei ^{63}Ga and ^{65}Ga were studied following the reaction ^{32}S + ^{40}Ca at a reaction energy of 125 MeV and using the GASP γ-ray spectrometer in combination with the ISIS charged-particle detector system. In addition to low-lying negative-parity states with single-particle character, rotational-like cascades built on the $9/2^+$ and $19/2^-$ states have been observed in both nuclei. Sidebands with negative parity in ^{63}Ga and positive parity in ^{65}Ga could be established. The experimental results are compared with Total Routhian Surface calculations which describe the nuclei as moderately deformed ($\beta_2 \approx 0.25$) and γ soft at low rotational frequencies. The highest experimentally observed positive-parity state in ^{65}Ga ($41/2^+$) is in good agreement with the calculated crossing of the collective band with a non-collective one terminating at this spin.

PACS. 21.60.Ev Collective models – 23.20.En Angular distribution and correlation measurements – 23.20.Lv Gamma transitions and level energies – 27.50.+e $59 \leq A \leq 89$

1 Introduction

The low- to medium-spin states in the doubly magic nucleus ^{56}Ni and its nearby neighbours [1] show single-particle excitations which can well be interpreted in terms of the spherical shell model. Following the $N = Z$ line towards higher masses, the light Kr and Sr isotopes show collective properties with a strong dependence of the deformation parameters on the number of nucleons (see, for example, [2,3]). The neutron-deficient Ga isotopes fall in the transitional region between these two domains. Thus, excitation in these nuclei occurs as an interplay between single-particle states and collective states with prolate or oblate deformation. With respect to the doubly magic $N = Z = 28$ core ^{56}Ni, the isotopes ^{63}Ga and ^{65}Ga have three valence protons and four and six valence neutrons, respectively. In the spherical case and for low excitation energies these valence particles occupy the negative parity $p_{3/2}$ and $f_{5/2}$ orbitals. Consequently, the light odd-A Ga isotopes have negative-parity ground states: $I^\pi = 3/2^-$, and $5/2^-$ states have been identified as lowest excited levels in ^{63}Ga [4], ^{65}Ga, and ^{67}Ga [5]. Other low-lying negative-parity states have been interpreted by the coupling of the odd proton to the 0^+ or 2^+ states in the respective even-even cores ^{62,64,66}Zn.

On the other hand, collective states are favoured by the energy gap in the Nilsson diagram at $N, Z = 34, 36$ for oblate deformation and $N, Z = 38$ for prolate deformation. Here, the occupation of the positive-parity $g_{9/2}$ intruder orbital plays an important role for the structure of excited states. In the odd-A Ga isotopes, the $9/2^+$ levels at about 2.0 MeV excitation energy with all probability originate from the promotion of the unpaired proton into the $g_{9/2}$ orbital. These states mark the band head of positive-parity cascade in the respective nucleus. Higher spin values in these bands are then obtained by the alignment of one $g_{9/2}$ neutron pair.

Recently, excited states in the odd-odd $N = Z$ nucleus ^{62}Ga have been identified [6,7] and studied theoretically within the framework of the spherical shell model as well as the cranked Nilsson-Strutinsky model [8].

[a] e-mail: matthias@tsl.uu.se
[b] *Present address:* Defense Research Establishment (FOA), 172 90 Stockholm, Sweden.

In this paper, we present results on the odd-A isotopes ^{63}Ga and ^{65}Ga.

2 Experimental procedure and results

Experimental details

An experiment aiming at a detailed study of high-spin states in ^{64}Ge [9,10] and neighbouring nuclei was performed at the Tandem XTU accelerator at the Legnaro National Laboratory in Legnaro, Italy. The target consisted of a 0.4 mg/cm^2 thick ^{40}Ca layer on a 3 mg/cm^2 thick Au backing. From the other side, the Ca surface was protected against oxidation by a 50 μg/cm^2 thin Au film. To prevent Doppler broadening of the γ-ray transitions due to a varying velocity of the emitting nucleus, the target was mounted with the backing facing the beam. This target was bombarded with a 140 MeV ^{32}S beam. In the backing, the beam energy was reduced to a reaction energy of about 125 MeV. The nuclei discussed in this paper were populated by the reactions ^{40}Ca(^{32}S, $2\alpha p$)^{63}Ga and ^{40}Ca(^{32}S, $\alpha 3p$)^{65}Ga, respectively.

The γ-radiation was detected in the 4 π γ-ray spectrometer GASP [11] containing 40 Compton suppressed large-volume Ge detectors and an 80 segment BGO multiplicity filter. The distance of the Ge detectors from the target was 28 cm, resulting in a photopeak efficiency of 3% at 1.3 MeV γ-ray energy. The Ge detectors were mounted in seven rings under average angles of 35° (145°), 59° (121°), 72° (108°), and 90° with respect to the beam axis. This geometry allows to measure γ-ray angular distributions and correlations.

A distinction of the various reaction channels after the formation of the compound nucleus was done on the basis of charged-particle detection in the 40 element Si-ball ISIS [12]. Each element consists of a 130 μm thin ΔE and a 1000 μm thick E detector. To protect the Si detectors against the beam, the elements were shielded with Al absorbers. Sorting the ISIS signals off-line into $\Delta E - E$ matrices allowed for a good separation between protons, α-particles, and double-hits by means of two-dimensional gates. With the used absorbers and electronic thresholds and the chosen gates for the charged particles, an identification efficiency of 35% for protons and 21% for α-particles was achieved.

An event was qualified by the coincidence of at least two Compton suppressed γ-rays in the Ge detectors and three γ-rays in the multiplicity filter. In total, 10^9 events were recorded. The energy calibration of the Ge detectors was done with ^{152}Eu, ^{133}Ba, and ^{56}Co sources. A comparison of peak positions at different detector angles yielded an average velocity of the recoiling nuclei of $v/c = 3.7\%$. A Doppler correction of the γ-ray energies was carried out on an event-by-event basis. This correction includes a kinematics correction to account for the change of the velocity of the residual nucleus due to the emission of the detected charged particles. γ-rays were accepted as belonging to ^{63}Ga if either two α particles or two α-particles and one proton were detected. For ^{65}Ga, the detection of one α-particle and three protons was required.

To determine the spins of excited states, DCO ratios (Directional Correlations from Oriented states [13]) of a number of transitions have been measured. The DCO ratio is defined as

$$R_{\mathrm{DCO}} = \frac{I(\gamma_1 \text{ at } \Theta_1 \text{ gated by } \gamma_2 \text{ at } \Theta_2)}{I(\gamma_1 \text{ at } \Theta_2 \text{ gated by } \gamma_2 \text{ at } \Theta_1)}, \quad (1)$$

where the gate is set on a transition with known multipolarity. For the GASP geometry, $\gamma\gamma$ correlations between detectors in the rings at $\Theta_1 = 35°$ (145°) with 12 detectors and the ring at $\Theta_2 = 90°$ (8 detectors) have been analysed. When gating on a stretched quadrupole transition, the DCO ratio is $R_{\mathrm{DCO}} = 1.0$ for a stretched quadrupole and $R_{\mathrm{DCO}} \approx 0.5$ for a stretched dipole transition. For dipole transitions with $\Delta I = 0$ and small mixing ratios ($|\delta| < 0.5$), the DCO ratio becomes $R_{\mathrm{DCO}} \approx 1.0$.

In order to take profit from the full efficiency of the GASP spectrometer, the angular restriction for the gating transition can be released. Instead of an angular correlation, the measured quantity then is a "gated" angular distribution, defined by the ADO ratio (Angular Distributions from Oriented states [14])

$$R_{\mathrm{ADO}} = \frac{I(\gamma_1 \text{ at } \Theta_1 \text{ gated by } \gamma_2)}{I(\gamma_1 \text{ at } \Theta_2 \text{ gated by } \gamma_2)}, \quad (2)$$

with $\Theta_1 = 35°$ (145°) and $\Theta_2 = 90°$. The coincidence yields have to be corrected for the different detection efficiencies at the corresponding angles. The ADO ratios are about $R_{\mathrm{ADO}} \approx 1.1$ for a stretched quadrupole and $R_{\mathrm{ADO}} \approx 0.6$ for a stretched dipole transition.

In a further step, angular correlations can be used to determine the nuclear alignment and the multipole mixing ratios δ of transitions. For this purpose, angular correlation values as defined by

$$W_{\mathrm{DCO}} = I(\gamma_1 \text{ at } \Theta_1 \text{ gated by } \gamma_2 \text{ at any other } \Theta_2) \quad (3)$$

have been formed for $\Theta_1 = 35°$, 59°, 72°, and 90°. The corresponding theoretical value is given by [13]

$$W(\Theta_1, \Theta_2, \Phi) = \sum_{\lambda_1 \lambda \lambda_2} B_{\lambda_1}(I_1) A_{\lambda}^{\lambda_2 \lambda_1}(X_1) A_{\lambda_2}(X_2) \times \frac{4\pi}{2\lambda_2 + 1} \sum_q \langle \lambda_1 0 \lambda q | \lambda_2 q \rangle Y_{\lambda q}(\Theta_1, 0) Y^*_{\lambda_2 q}(\Theta_2, \Phi). \quad (4)$$

For a comparison with the experimental data, an additional summation over all possible angles Φ between the two involved detectors has to be performed. The orientation parameters $B_{\lambda_1}(I_1)$ depend on the initial alignment of the state I_1, the radiation distribution parameters $A_{\lambda}^{\lambda_2 \lambda_1}(X_1)$ and $A_{\lambda_2}(X_2)$ on the multipolarity and the mixing ratio of the respective transition. In case of known mixing ratios (*e.g.*, within a cascade of stretched $E2$ transitions, $\delta_1(M3/E2) = \delta_2(M3/E2) = 0$) the initial alignment of the residual nucleus can be determined. For nuclei produced in heavy-ion compound nucleus reactions,

the population parameters for the nuclear substates for a given spin can be represented by a Gaussian distribution [15]. As a consequence, the alignment parameter α_4 is a unique function of α_2, which thus is the only free parameter in the fit. On the other hand, the knowledge of the alignment allows to deduce the mixing ratio of one of the transitions if the other one is known (*e.g.*, $\delta(M2/E1)$ or $\delta(E2/M1)$ for an $E2$-$E1$ or $E2$-$M1$ cascade, respectively). The absence of detectors at $\Theta \approx 0°$ in the GASP geometry prohibits the precise determination of these values. However, this procedure provides a valuable aid when judging the electric or magnetic nature of stretched dipole transitions.

Level scheme of ^{63}Ga

The ground-state spin and parity of ^{63}Ga are tentatively known from β-decay studies [16]. The allowed decay of ^{63}Ga to the $3/2^-$ and $5/2^-$ states in ^{63}Zn demands a $3/2^-$ or $5/2^-$ ground state of the ^{63}Ga mother nucleus. In the spherical limit, the unpaired proton in ^{63}Ga occupies the $2p_{1/2}$ subshell. This consideration as well as the systematics of odd-mass Ga isotopes led the authors of [16] to the spin-parity assignment of $I^\pi = 3/2^-$ for the ground state in ^{63}Ga.

A previous study [4] resulted in a level scheme for ^{63}Ga based on neutron-γ, charged-particle-γ, and $\gamma\gamma$ coincidences. The authors established yrast states up to a probable spin of about 23/2 at an excitation energy of 7.7 MeV.

Since the ground-state spin and parity in ^{63}Ga have not been unambiguously determined and only spin differences have been deduced in the present experiment, all absolute spin values have to be considered as tentative. However, for the following discussion as well as in all tables and figures, brackets have been omitted if the spin difference to the ground state is well established and set just in cases of insecure spin differences. The level scheme of ^{63}Ga, as obtained in the present work, is shown in fig. 1, energies, γ-ray intensities, spins, ADO-, and DCO-ratios are summarised in table 1.

The decay of the $9/2^+$ band head of the positive-parity cascade at $E_x = 2047$ keV is dominated by the 894 keV-1077 keV-75 keV cascade ($9/2^+ \rightarrow 9/2^- \rightarrow 5/2^- \rightarrow 3/2^-$) and the 625 keV-1423 keV sequence ($9/2^+ \rightarrow 7/2^- \rightarrow 3/2^-$) [4]. Parallel to the 1423 keV transition, two sequences and one interconnecting transition could be established. Due to the uncertainties in the intensities, the order of these transitions could not be determined unambiguously. Furthermore, the intensity of the 625 keV transition is about the same as the summed intensities of the 1423 keV transition and its parallel sequences, see table 1. However, an analysis of the intensities of all feeding and depopulating transitions in cuts on all involved transitions results in a reversion of the order of the 1423 keV and the 625 keV transitions as compared to the level scheme in ref. [4]. The ADO ratio of the 1423 keV line ($R_{\mathrm{ADO}} = 0.95(5)$) establishes it as a quadrupole transition, whereas the DCO and ADO ratios for the 625 keV

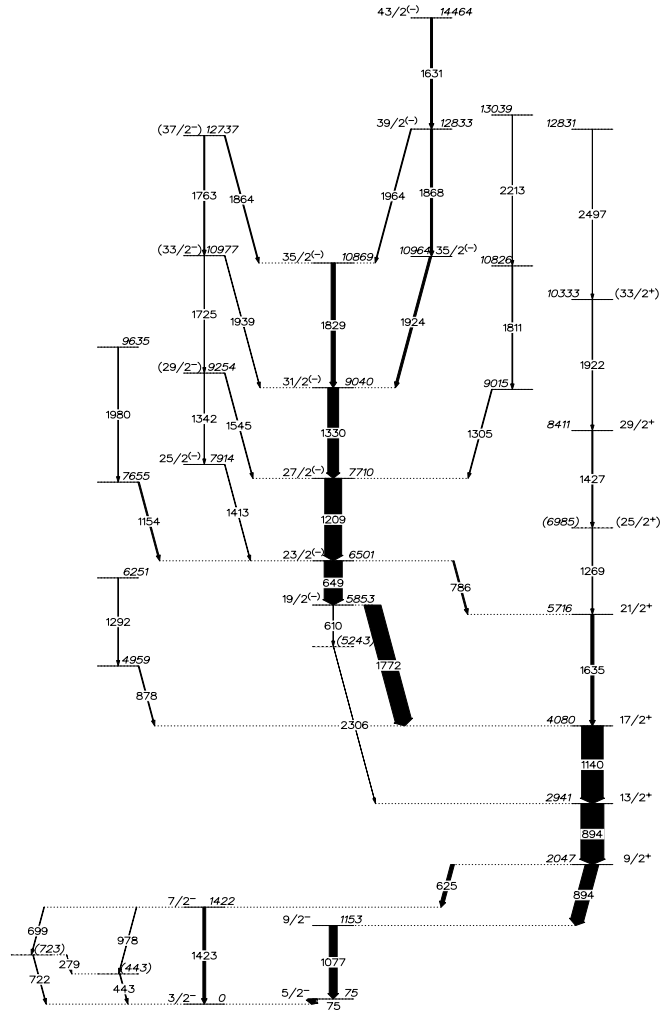

Fig. 1. Level scheme of ^{63}Ga as obtained in the present work. The thickness of the lines indicates the γ-ray intensity. All energies are given in keV.

line ($R_{\mathrm{DCO}} = 0.63(9)$, $R_{\mathrm{ADO}} = 0.77(4)$) indicate stretched dipole character. Thus, spin and parity of $I^\pi = 7/2^-$ is assigned to the intermediate state. The quadrupole nature of the 1077 keV line has been measured in [4] and could be confirmed. The measured DCO and ADO ratios for the 894 keV doublet ($13/2^+ \rightarrow 9/2^+$ and $9/2^+ \rightarrow 9/2^-$) are compatible with the assignment of one quadrupole and one non-stretched dipole component.

The positive-parity band, based on the $9/2^+$ state, has been observed up to 12831 keV excitation energy. Spins could be determined up to the $(33/2^+)$ state at $E_x = 10.3$ MeV, which is connected to the $9/2^+$ state via a sequence of stretched quadrupole transitions. The order of the 1269 keV and 1427 keV transitions which connect the $29/2^+$ and the $21/2^+$ states has been determined on the basis of the intensities in the cut on the 1140 keV $17/2^+ \rightarrow 13/2^+$ and the 1635 keV $21/2^+ \rightarrow 17/2^+$ transitions. However, in the $\gamma\gamma$ projection the 1427 keV transition appears more intense than the 1269 keV line (see table 1). For this reason, the order of these transitions is assigned tentatively. Due to the doublet structure of the 1922 keV

Table 1. Level and transition energies, intensities, DCO-ratios and level spins in ^{63}Ga.

E_x (keV)	E_γ (keV)		$Y_{\rm rel}$		$R_{\rm DCO}$		$R_{\rm ADO}$		$I_{\rm i}^{\pi}$	$I_{\rm f}^{\pi}$
75.3(2)	75.2	(2)							$5/2^-$	$3/2^-$
443.2(3)	443.1	(2)	2.5	(2)						$3/2^-$
722.5(4)	722.2	(2)	2.6	(7)						$3/2^-$
	279.2	(4)	0.2	(1)						
1152.6(3)	1077.2	(2)	34.6	(15)	0.93	(8)[a]	1.01	(2)[a]	$9/2^-$	$5/2^-$
1422.0(3)	1422.6	(2)	12.3	(7)			0.95	(5)[a]	$7/2^-$	$3/2^-$
	978.4	(2)	2.2	(1)					$7/2^-$	
	699.3	(2)	2.4	(1)					$7/2^-$	
2046.5(3)	893.7	(2)	57.5	(19)	1.07	(4)[b,c]	1.05	(1)[b,c]	$9/2^+$	$9/2^-$
	624.6	(2)	16.1	(5)	0.63	(9)[a]	0.77	(4)[a]	$9/2^+$	$7/2^-$
2940.6(5)	894.0	(2)	100.0	(31)	1.07	(4)[b,c]	1.05	(1)[b,c]	$13/2^+$	$9/2^+$
4080.4(5)	1139.9	(2)	93.9	(29)	0.97	(7)[d]	1.17	(4)[d]	$17/2^+$	$13/2^+$
4958.8(10)	878.4	(2)	3.3	(2)						$17/2^+$
5243.3(14)	2306.0	(7)	0.6	(5)						$13/2^+$
5715.5(7)	1634.9	(2)	13.3	(5)	1.36	(17)[c]	1.30	(6)[c]	$21/2^+$	$17/2^+$
5852.7(6)	1772.3	(2)	71.8	(22)	0.55	(4)[c]	0.60	(1)[c]	$19/2^-$	$17/2^+$
	609.6	(3)	0.9	(1)					$19/2^-$	
6251.0(22)	1292.1	(4)	1.5	(1)						
6501.4(6)	785.7	(2)	6.3	(2)	0.68	(9)[e]	0.67	(3)[e]	$23/2^-$	$21/2^+$
	648.7	(2)	78.8	(24)	1.09	(5)[c]	1.13	(2)[c]	$23/2^-$	$19/2^-$
6984.7(11)	1269.2	(2)	2.9	(2)			0.94	(3)[c]	$25/2^+$	$21/2^+$
7655.0(9)	1153.6	(2)	5.8	(2)						$23/2^-$
7710.3(7)	1208.9	(2)	73.7	(22)	1.12	(5)[f]	1.20	(2)[f]	$27/2^-$	$23/2^-$
7914.3(16)	1413.4	(3)	2.3	(1)			0.38	(3)[f]	25/2	$23/2^-$
8411.3(14)	1426.6	(2)	4.4	(4)			1.22	(12)[c]	$29/2^+$	$25/2^+$
9014.9(12)	1304.6	(2)	3.2	(1)						
9040.0(7)	1329.7	(2)	47.2	(14)	1.15	(7)[f]	1.28	(3)[f]	$31/2^-$	$27/2^-$
9254.4(12)	1544.7	(3)	2.9	(1)					(29/2)	$27/2^-$
	1341.9	(5)	1.0	(1)					(29/2)	25/2
9635.0(17)	1980.0	(3)	2.4	(1)						
10333.2(23)	1921.9	(4)	2.4	(1)			1.05	(9)[a,b]	$(33/2^+)$	$29/2^+$
10826.3(16)	1811.5	(3)	3.2	(1)						
10869.0(8)	1828.6	(2)	18.2	(6)	1.08	(12)[g]	1.22	(4)[g]	$35/2^-$	$31/2^-$
10964.3(9)	1924.3	(2)	9.6	(3)			1.02	(6)[h]	$35/2^-$	$31/2^-$
10976.6(12)	1939.5	(3)	2.2	(1)					(33/2)	$31/2^-$
	1725.4	(4)	1.1	(1)					(33/2)	(29/2)
12737.0(13)	1864.0	(3)	4.0	(2)			0.40	(2)[b,g]	(37/2)	$35/3^-$
	1763.5	(3)	4.3	(2)					(37/2)	(33/2)
12831(4)	2497.4	(6)	0.9	(3)						
12832.6(9)	1963.6	(2)	3.6	(1)			0.93	(6)[g]	$39/2^-$	$35/2^-$
	1868.3	(2)	9.1	(3)			0.40	(2)[b,g]	$39/2^-$	$35/2^-$
13039(4)	2213.0	(6)	0.7	(1)						
14463.5(11)	1631.0	(2)	8.5	(3)			1.25	(8)[h]	$43/2^-$	$39/2^-$

a) Gate on 1140 keV.
b) Both components of the doublet.
c) Gate on 1077 keV and 1140 keV.
d) Gate on 1077 keV.
e) Gate on 1077 keV, 1140 keV, and 1209 keV.
f) Gate on 1077 kev, 1140 keV, and 649 keV.
g) Gate on 1077 keV, 1140 keV, 649 keV, and 1209 keV.
h) Gate on 649 keV and 1209 keV.

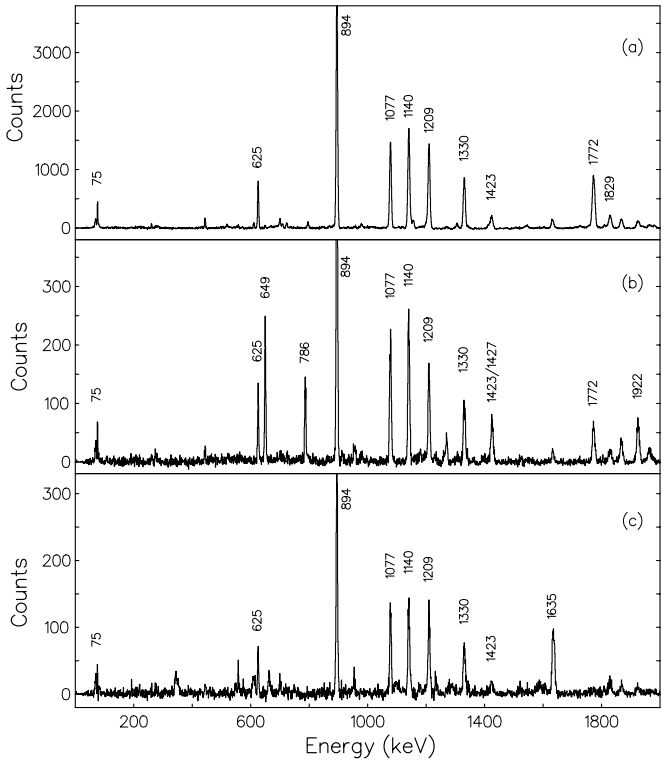

Fig. 2. γ-ray spectra from the reaction ^{40}Ca(^{32}S,2αp)^{63}Ga gated by two α-particles. The energies are labelled in keV. (a) Gate on the 649 keV $23/2^{(-)} \rightarrow 19/2^{(-)}$ transition. (b) Gate on the 1635 keV $21/2^{+} \rightarrow 17/2^{+}$ transition. (c) Gate on the 786 keV $23/2^{(-)} \rightarrow 21/2^{+}$ transition.

line (1924 keV, $35/2^{-} \rightarrow 31/2^{-}$) and the low statistics in the positive-parity branch, an unambiguous spin assignment of the $(33/2^{+})$ state has not been possible.

Above the $17/2^{+}$ state at $E_x = 4080$ keV, the main γ-intensity flux is carried via the 1772 keV and 649 keV transitions to a cascade of stretched quadrupole ($E2$) transitions. In contrast to the level scheme published in [4] and despite of the slightly higher γ intensity of the 649 keV line (79(2)% compared to 72(2)% of the 1772 keV line) determined from the $\gamma\gamma$ projection, the 1772 keV transition has been placed below the 649 keV line. This is based on the relative intensities in cuts on the 1140 keV, 1772 keV, and 649 keV lines and confirmed by the identification of the 610 keV and 2306 keV transitions which were found parallel to the 1772 keV-1140 keV sequence. The DCO and ADO ratios for the 1772 keV line show that this is a stretched dipole transition. The 649 keV line displays quadrupole character.

Parallel to the 649 keV-1772 keV cascade, a sequence of two transitions with 786 keV and 1635 keV, also connecting the $23/2^{(-)}$ and the $17/2^{+}$ states, has been identified. Spectra with gates on these two transitions are displayed in fig. 2. The peaks at 649 keV and 1772 keV in the cut on the 1635 keV transition are due to the doublet structure of this line with the second component being the 1631 keV $43/2^{(-)} \rightarrow 39/2^{(-)}$ transition. The high intensity of the 1922 keV $(33/2^{+}) \rightarrow 29/2^{+}$ line as compared to the 1269 keV $(25/2^{+}) \rightarrow 21/2^{+}$ transition can as well be explained by this doublet and the resulting coincidence between the 1631 keV $43/2^{(-)} \rightarrow 39/2^{(-)}$ and the 1924 keV $35/2^{(-)} \rightarrow 31/2^{(-)}$ transition.

The $E2$ cascade that starts with the 649 keV transition and reaches up to an excitation energy of $E_x = 14.5$ MeV can be used to determine the nuclear alignment. For this, the DCO values $W_{\rm DCO}$ (see eq. 3) are calculated from the experimental data for the $27/2 \rightarrow 23/2 \rightarrow 19/2$ and the $31/2 \rightarrow 27/2 \rightarrow 23/2$ sequences and compared to the theoretical values for different initial alignments. Figure 3 shows the experimental results for the $27/2 \rightarrow 23/2 \rightarrow 19/2$ cascade in comparison with calculations for initial alignments between $\alpha_2 = 0.5$ and $\alpha_2 = 0.8$. For $E2$ transitions, the mixing ratio is practically zero and the only free parameter is the initial nuclear alignment. A χ^2 analysis yields a result of $\alpha_2 = 0.6(1)$.

With this value for the alignment it is possible to determine the mixing ratio for the 1772 keV $19/2 \rightarrow 17/2$ transition from the angular correlation between this line and either the 649 keV or the 1140 keV $E2$ transition. This is illustrated in fig. 4 for the $19/2 \rightarrow 17/2 \rightarrow 13/2$ cascade. Calculations for different mixing ratios for the 1772 keV transition show best agreement for small negative mixing ratios $\delta = -0.3(2)$. This result is compatible with an $E1$ assignment to the 1772 keV transition. For this reason, the 19/2 state is suggested to have negative parity, which, however, is considered as tentative. The cascade built on it reaches up to spin $35/2^{(-)}$. A second $35/2^{(-)}$ state has been identified only 95 keV above the yrast state. Based

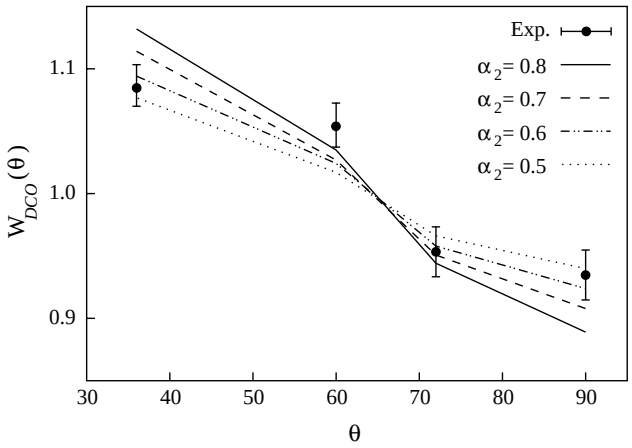

Fig. 3. DCO values for the $27/2^- \rightarrow 23/2^- \rightarrow 19/2^-$ cascade in ^{63}Ga. Displayed are the experimental values for the four GASP detector angles and calculated ones for different alignment parameters α_2.

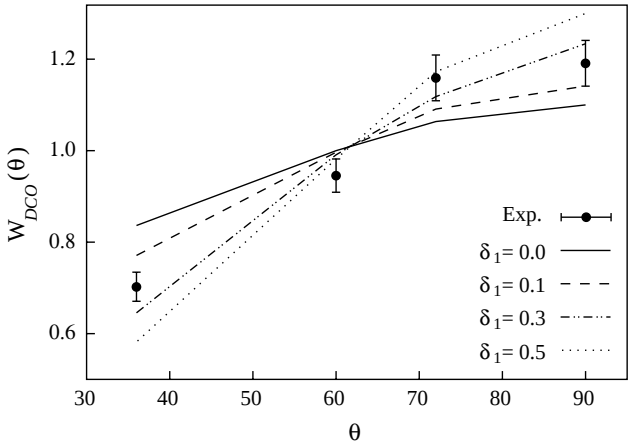

Fig. 4. DCO values for the $19/2^- \rightarrow 17/2^- \rightarrow 13/2^-$ cascade in ^{63}Ga. Experimental values are compared with calculations for different mixing ratios δ for the $19/2^- \rightarrow 17/2^+$ transition.

on it, another cascade reaching up to spin $43/2^{(-)}$ was found.

The 1342 keV, 1725 keV, and 1763 keV transitions form a sideband to the negative-parity cascade, which extends from an excitation energy of $E_x = 7914$ keV to $E_x = 12737$ keV. Within this sideband, no multipolarities could be determined. The measured ADO ratio for the 1413 keV transition which depopulates the band head, $R_{\mathrm{ADO}} = 0.38(3)$, determines the spin of the 7914 keV level to be 25/2. The decay pattern of the other states in this cascade, in-band transitions and high-energy transitions feeding the $27/2^{(-)}$, $31/2^{(-)}$, and $35/2^{(-)}$ levels, allows to assume dipole character also for the other transitions depopulating the band and thus quadrupole transitions inside the cascade. This way, tentative spin values of (29/2), (33/2), and (37/2) have been assigned to the 9254 keV, 10977 keV, and 12737 keV levels, respectively. Since the levels in this cascade decay exclusively into negative-parity states, tentative negative parity is also assigned to this sideband.

A few more side structures have been placed into the level scheme. Due to the low statistics of the transitions it was, however, not possible to determine any spins for these states.

Level scheme of ^{65}Ga

The ground-state spin and parity in ^{65}Ga, $I^\pi = 3/2^-$, has been established on the basis of radioactive-decay studies [17] and proton transfer reactions [18,19], which also yielded information about low-lying levels. Prior to the present study, the most comprehensive study on high-spin states in ^{65}Ga was done by Dankó *et al.* [5]. From the reaction ^{58}Ni on ^{12}C at a beam energy of 261 MeV these authors obtained a level scheme for ^{65}Ga reaching up to an excitation energy of 8.6 MeV with assigned spin values up to a 27/2 state. One weakly populated cascade connecting the $17/2^+$ and the $9/2^+$ states, a negative-parity

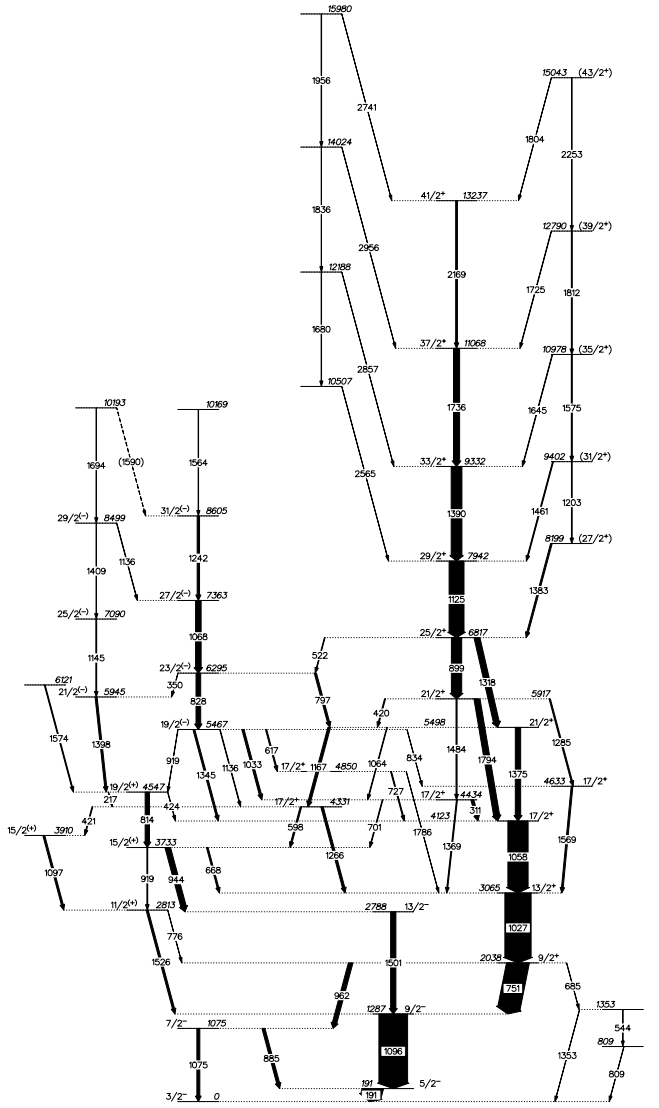

Fig. 5. Level scheme of ^{65}Ga as obtained in the present work. The thickness of the lines indicates the γ-ray intensity. All energies are given in keV.

Table 2. Level and transition energies, intensities, DCO-ratios and level spins in ^{65}Ga.

E_x (keV)	E_γ (keV)	$Y_{\rm rel}$	$R_{\rm DCO}$	$R_{\rm ADO}$	$I_{\rm i}^{\pi}$	$I_{\rm f}^{\pi}$
190.8(1)	190.8 (1)	100.0 (29)	0.82 (2)[a]	0.68 (1)[b]	$5/2^-$	$3/2^-$
808.8(8)	809.3 (2)	1.0 (2)				$3/2^-$
1075.3(2)	1075.2 (1)	9.6 (4)		1.09 (5)[c]	$7/2^-$	$3/2^-$
	884.6 (1)	9.7 (3)		0.75 (4)[c]	$7/2^-$	$5/2^-$
1286.9(2)	1096.2 (1)	93.6 (28)	0.77 (4)[c]	0.94 (2)[c]	$9/2^-$	$5/2^-$
1353.0(6)	1352.9 (4)	0.9 (1)				$3/2^-$
	544.4 (2)	0.5 (1)				
2037.7(2)	962.3 (1)	14.5 (4)	0.67 (4)[c]	0.68 (2)[c]	$9/2^+$	$7/2^-$
	750.9 (1)	73.4 (22)	1.16 (5)[b]	1.08 (2)[b]	$9/2^+$	$9/2^-$
	684.8 (1)	0.8 (1)			$9/2^+$	
2788.5(2)	1501.5 (1)	17.2 (5)	0.94 (9)[b]	1.04 (5)[b]	$13/2^-$	$9/2^-$
2813.4(3)	1526.3 (1)	6.8 (2)		0.66 (3)[d]	$11/2^{(+)}$	$9/2^-$
	775.7 (2)	0.8 (1)			$11/2^{(+)}$	$9/2^+$
3064.7(2)	1027.1 (1)	85.6 (26)	1.28 (8)[b]	1.23 (4)[b]	$13/2^+$	$9/2^+$
3732.8(2)	944.3 (1)	17.8 (5)	0.60 (3)[e]	0.69 (2)[e]	$15/2^{(+)}$	$13/2^-$
	919.1 (1)	2.6 (1)		1.05 (6)[d]	$15/2^{(+)}$	$11/2^{(+)}$
	668.3 (1)	5.1 (2)		0.68 (4)[a]	$15/2^{(+)}$	$13/2^+$
3910.1(3)	1096.6 (1)	6.2 (3)			$15/2^{(+)}$	$11/2^{(+)}$
4122.8(3)	1057.9 (1)	65.9 (20)	1.12 (4)[a]	1.13 (2)[a]	$17/2^+$	$13/2^+$
4330.7(3)	1266.0 (1)	7.7 (2)	0.92 (9)[a]	1.18 (7)[a]	$17/2^+$	$13/2^+$
	597.9 (1)	4.6 (1)			$17/2^+$	$15/5^{(+)}$
	420.7 (1)	2.6 (1)		0.79 (4)[e]	$17/2^+$	$15/2^+$
4433.6(3)	1369.2 (1)	3.2 (1)		1.39 (11)[a]	$17/2^+$	$13/2^+$
	700.7 (1)	2.2 (1)		0.51 (5)[e]	$17/2^+$	$15/2^{(+)}$
	310.8 (1)	9.5 (3)	1.22 (6)[f]	1.15 (3)[f]	$17/2^+$	$17/2^+$
4547.1(3)	814.4 (1)	14.1 (4)	1.17 (8)[e]	1.21 (4)[e]	$19/2^{(+)}$	$15/2^{(+)}$
	424.2 (1)	1.3 (1)			$19/2^{(+)}$	$17/2^+$
	216.4 (1)	1.2 (1)			$19/2^{(+)}$	$17/2^+$
4632.8(3)	1568.5 (1)	5.5 (2)		1.18 (6)[a]	$17/2^+$	$13/2^+$
4850.1(3)	1785.8 (3)	0.7 (1)			$17/2^+$	$13/2^+$
	727.3 (1)	3.1 (1)		1.10 (6)[f]	$17/2^+$	$17/2^+$
5467.1(3)	1344.6 (1)	5.9 (2)		0.56 (2)[g]	$19/2^-$	$17/2^+$
	1136.1 (2)	1.8 (1)			$19/2^-$	$17/2^+$
	1033.4 (1)	7.1 (2)	0.64 (4)[g]	0.67 (3)[g]	$19/2^-$	$17/2^+$
	919.2 (2)	0.9 (1)			$19/2^-$	$19/2^{(+)}$
	834.4 (2)	0.6 (1)			$19/2^-$	$17/2^+$
	616.9 (1)	3.8 (1)		0.50 (3)[f]	$19/2^-$	$17/2^+$
5497.9(3)	1375.1 (1)	17.5 (5)	1.03 (5)[f]	1.04 (3)[f]	$21/2^+$	$17/2^+$
	1167.1 (1)	8.6 (3)		0.97 (6)[a]	$21/2^+$	$17/2^+$
	1063.7 (2)	2.1 (1)			$21/2^+$	$17/2^+$

a) Gate on 1096 keV and 1027 keV.
b) Gate on 1096 keV.
c) Gate on 1027 keV and 1058 keV.
d) Gate on 1096 keV and 814 keV.
e) Gate on 1096 keV and 1501 keV.
f) Gate on 1096 keV, 1027 keV, and 1058 keV.
g) Gate on 1096 keV, 1027 keV, 1058 keV, and 828 keV.
h) Gate on 1096 keV, 1501 keV, and 814 keV.
i) Gate on 1096 keV, 1027 keV, 1058 keV, and 1375 keV.
j) Gate on 1096 keV, 1027 keV, 1058 keV, and 1125 keV.
k) Gate on 1125 keV and 1390 keV.
l) Gate on 1096 keV, 1027 keV, 1058 keV, 1125 keV, and 1390 keV.

Table 2. *Continued.*

E_x (keV)	E_γ (keV)		$Y_{\rm rel}$		$R_{\rm DCO}$		$R_{\rm ADO}$		$I_{\rm i}^{\pi}$	$I_{\rm f}^{\pi}$
5917.2(3)	1794.0	(1)	19.6	(6)	0.84	$(5)^f$	1.17	$(3)^f$	$21/2^+$	$17/2^+$
	1484.0	(1)	3.4	(1)					$21/2^+$	$17/2^+$
	1284.7	(1)	4.1	(1)			1.18	$(10)^a$	$21/2^+$	$17/2^+$
	419.6	(1)	3.1	(1)					$21/2^+$	$21/2^+$
5944.8(3)	1397.9	(1)	6.6	(2)			0.61	$(2)^h$	$21/2^{(-)}$	$19/2^+$
6121.3(6)	1574.2	(1)	2.9	(1)						$19/2^{(+)}$
6295.1(3)	828.0	(1)	15.3	(5)	0.95	$(6)^f$	1.00	$(3)^f$	$23/2^-$	$19/2^-$
	797.3	(1)	7.1	(2)			0.70	$(3)^f$	$23/2^-$	$21/2^+$
	350.5	(1)	1.0	(1)					$23/2^-$	$21/2^{(-)}$
6816.5(3)	1318.5	(1)	19.1	(6)	1.01	$(10)^i$	1.29	$(8)^f$	$25/2^+$	$21/2^+$
	899.4	(1)	33.7	(10)	1.31	$(6)^f$	1.35	$(3)^f$	$25/2^+$	$21/2^+$
	521.6	(1)	2.2	(1)					$25/2^+$	$23/2^-$
7089.6(5)	1144.8	(1)	2.6	(1)			1.27	$(8)^h$	$25/2^{(-)}$	$21/2^{(-)}$
7362.9(3)	1067.8	(1)	18.2	(6)	0.82	$(6)^i$	1.24	$(5)^a$	$27/2^-$	$23/2^-$
7941.7(3)	1125.2	(1)	48.6	(15)	1.14	$(4)^f$	1.29	$(3)^f$	$29/2^+$	$25/2^+$
8199.3(5)	1382.7	(1)	5.2	(1)					$(27/2^+)$	$25/2^+$
8498.9(6)	1409.2	(1)	1.4	(1)			1.25	$(9)^h$	$29/2^{(-)}$	$25/2^{(-)}$
	1135.6	(2)	1.3	(1)					$29/2^{(-)}$	$27/2^-$
8605.0(4)	1242.1	(1)	7.7	(2)			1.13	$(4)^g$	$31/2^-$	$27/2^-$
9402.2(4)	1460.5	(1)	2.9	(1)					$(31/2^+)$	$29/2^+$
	1202.9	(1)	2.3	(1)					$(31/2^+)$	$(27/2^+)$
9331.8(4)	1390.0	(1)	35.0	(11)	1.10	$(4)^j$	1.24	$(3)^f$	$33/2^+$	$29/2^+$
10168.9(9)	1563.9	(2)	1.4	(1)						$31/2^-$
10192.7(9)	1693.6	(2)	1.4	(1)						$29/3^{(-)}$
	1589.6	(4)	0.4	(1)						$31/2^-$
10507.4(9)	2565.3	(5)	0.8	(3)						$29/2^+$
10977.5(5)	1644.9	(1)	1.6	(1)			0.36	$(3)^k$	$(35/2^+)$	$33/2^+$
	1575.3	(1)	3.1	(1)					$(35/2^-)$	$(31/2^-)$
11067.5(4)	1737.9	(1)	20.0	(6)	1.01	$(4)^l$	1.31	$(3)^l$	$37/2^+$	$33/2^+$
12188.0(9)	2857.3	(5)	0.7	(4)						$33/2^+$
	1680.4	(2)	1.3	(2)						
12790.3(6)	1812.3	(1)	2.9	(1)					$(39/2^+)$	$(35/2^+)$
	1724.6	(2)	1.4	(1)					$(39/2^+)$	$37/2^+$
13236.9(5)	2169.2	(2)	5.7	(2)	1.25	$(9)^l$	1.32	$(5)^l$	$41/2^+$	$37/2^+$
14024.1(10)	2956.2	(5)	0.6	(4)						$37/2^+$
	1836.3	(2)	0.9	(2)						
15043.4(8)	2253.5	(3)	1.5	(2)					$(43/2^+)$	$(39/2^+)$
	1804.2	(3)	0.7	(1)					$(43/2^+)$	$41/2^+$
15980.3(12)	2741.5	(9)	0.2	(2)						$41/2^+$
	1956.2	(2)	1.4	(2)						

band built on the $7/2^-$ state, and a few weak transitions, identified in [5] could not be observed in the present experiment. One sequence of transitions had to be reverted.

Due to the higher γ-ray efficiency of the GASP spectrometer as compared to the NORDBALL array used in [5] and because of the much higher angular momentum of the compound nuclei after the reaction ^{32}S + ^{40}Ca, a number of new bands developing at high excitation energies could be established in this work. Very recently, a partial level scheme for ^{65}Ga resulting from an experiment using the Euroball spectrometer has been presented [20]. These authors identified the main positive-parity band up to spin $41/2^+$ and two sidebands to this cascade. The negative-parity sequence could be extended as compared to the level scheme in [5]. Apart from one tentative line feeding the 15980 keV level and an additional decay out of one of the sidebands all states and transitions included in [20] have also been identified in the present work. Furthermore, a number of transitions mentioned neither in [5] nor in [20] could be established.

The level scheme of ^{65}Ga as deduced from this work is displayed in fig. 5. The γ-ray energies, intensities, ADO- and DCO-ratios as well as level energies and spins are summarised in table 2. Figure 6 shows examples of particle-gated γ-spectra. The low-lying states with negative parity and the positive-parity structure up to the $25/2^+$ state presented in [5] could be confirmed in the present analysis. The ground state of ^{65}Ga is populated mainly from the decay of the $9/2^+$ band head of the positive-parity structure via a $9/2^+ \rightarrow 9/2^- \rightarrow 5/2^- \rightarrow 3/2^-$ cascade. In

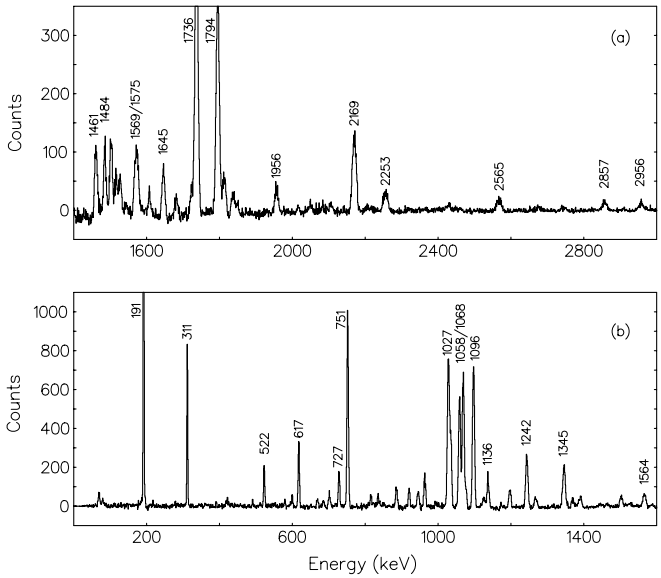

Fig. 6. γ-ray spectra from the reaction ^{40}Ca(^{32}S, $\alpha 3p$)^{65}Ga gated by one α-particle and three protons. The energies are labelled in keV. (a) Gate on 1125 keV. (b) Gate on 828 keV.

contrast to ^{63}Ga, where the positive-parity band continues up to spin $(33/2^+)$ without any side structures, two parallel cascades emerging from the $25/2^+$ state and feeding the $17/2^+$ state with comparable intensity have been observed in ^{65}Ga. Above the $25/2^+$ state, a sequence of stretched $E2$ transitions could be established reaching up to spin $41/2^+$ at an excitation energy of $E_x = 13.2$ MeV. Parallel to this sequence of positive-parity states and decaying into them, two sidebands have been identified. Due to the low relative intensity of the transitions inside and out of these bands, only the multipolarity of one transition connecting one of these side bands to the main positive-parity cascade could be determined. The 1645 keV transition populating the $33/2^+$ state has an ADO ratio of $R_{\rm ADO} = 0.36(3)$ and thus can be identified as dipole transition depopulating a $(35/2^+)$ state. The structure of this sideband and its decay to the main cascade allow tentative spin assignments also to the other states. The band reaches from spin $(27/2^+)$ to spin $(43/2^+)$ at an excitation energy of $E_x = 15.0$ MeV. The tentative assignment of positive parity is based on the partial decay of these states into the positive-parity band and on the lack of connections to any states with negative parity. The second side structure, connected to the main positive-parity band via four high-energy transitions ($E_\gamma \approx 2.5$–3 MeV) is too weakly populated to allow any spin assignments.

Below 5 MeV excitation energy it has been possible to assign positive parity to a number of levels. For the $17/2^+$ states at 4331 keV, 4434 keV, 4633 keV, and 4850 keV, this is based on their decay into the $13/2^+$ state and on their population from the $21/2^+$ state. For the $19/2^{(+)} \rightarrow 15/2^{(+)} \rightarrow 11/2^{(+)}$ cascade, positive parity can just tentatively be assigned, in agreement with the results in [5], but in contradiction to [21].

A state at 5467 keV excitation energy decays via stretched dipole transitions into several $17/2^+$ states. This determines the spin of this level to 19/2, in agreement to the results in [5], but the parity cannot be deduced from the present data. Due to the relatively high number of decay paths of the 19/2 state, an analysis of the mixing ratio for any depopulating dipole transition, as performed in ^{63}Ga, is not possible. Negative parity for this state is proposed on the basis of the measured ADO ratio for the $19/2^{(-)} \rightarrow 17/2^+$ transition ($R_{\rm ADO} = 0.56(2)$ as compared to $R_{\rm ADO} = 0.60(1)$ in ^{63}Ga) and because of the similarity of the decay patterns of ^{63}Ga and ^{65}Ga, but an experimental proof for this is still to be given. As compared to [5], the order of the 727 keV and 617 keV transitions depopulating the $19/2^{(-)}$ state has been reversed. The 1785 keV transition populating the intermediate state is now depopulating it and feeds the $13/2^+$ state. Based on the $19/2^{(-)}$ state, a sequence of three $E2$ transitions could be established, followed by a fourth transition of too low intensity to determine the multipolarity. One side structure to this band has been found. It is based on the $19/2^{(+)}$ state and consists of one dipole and two quadrupole transitions plus one of unknown multipolarity. Due to the connecting transitions between this side structure and the negative-parity states, negative parity is also suggested for this band.

3 Discussion

In [4], the excited states in ^{63}Ga were explained by single-particle excitations and their coupling to the even-even ^{62}Zn core. High-spin states in ^{65}Ga have been interpreted in the framework of the interacting boson fermion and broken pair model (IBFBPM) [5].

With respect to the higher spins observed in the present experiment and in order to gain comparable interpretations for both isotopes, we performed extended Total Routhian Surface (TRS) calculations [22]. In this

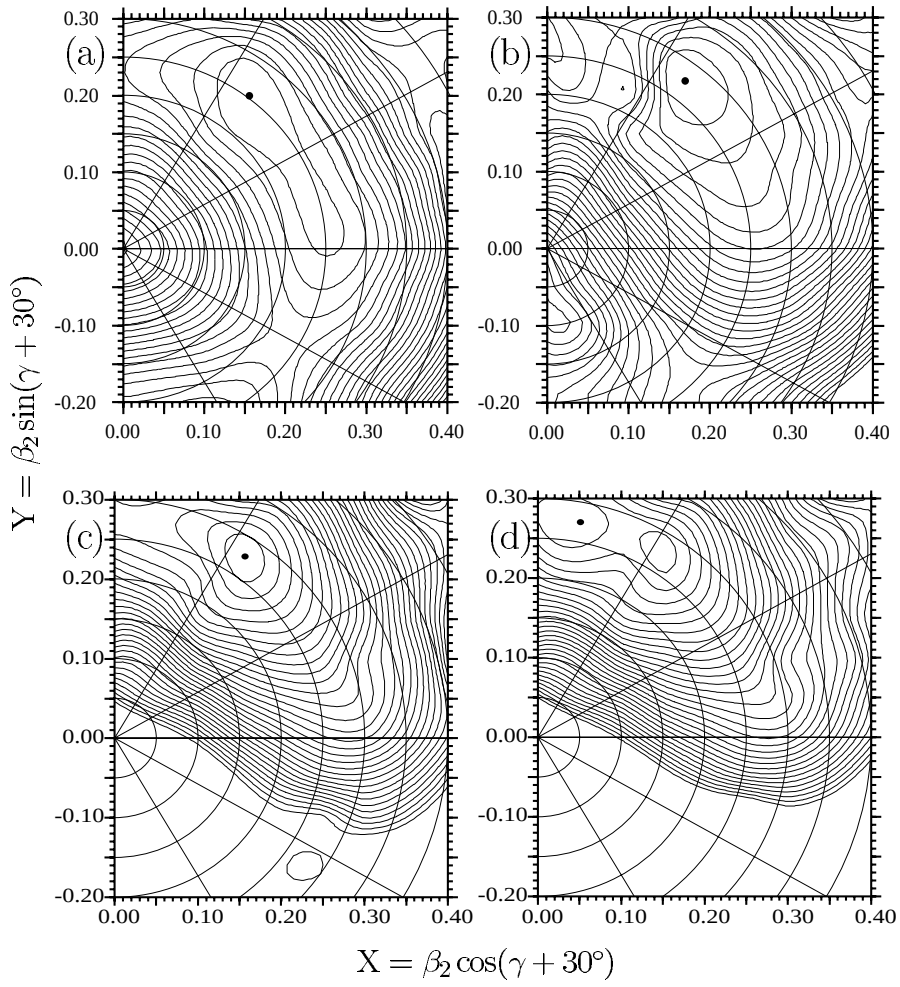

Fig. 7. Total Routhian Surfaces for positive and negative parity in ^{63}Ga. The (+,+1/2) configuration for $\hbar\omega = 0.0$ MeV (a) and $\hbar\omega = 0.8$ MeV (b) and the (–,–1/2) configuration for $\hbar\omega = 0.0$ MeV (c) and $\hbar\omega = 0.8$ MeV (d) are shown. The distance between the contour lines is 200 keV.

model, the nucleus is rotated externally about a fixed axis and the energy is calculated in this rotating frame of reference. The total Routhian contains the macroscopic liquid drop energy of the nucleus, a single-particle shell correction, and the pairing energy. The single-particle energies are obtained from a Woods-Saxon potential, the pairing includes a monopole and a double-stretched quadrupole interaction [23]. The Routhian is minimized with respect to the deformation parameters β_2, β_4, and γ.

In both nuclei, the $3/2^-$ ground state can be interpreted by the unpaired proton occupying a subshell emerging from the spherical the $p_{3/2}$ orbital. The low-lying $5/2^-$ state results from the promotion of the proton into the $f_{5/2}$ orbital. Other low-lying negative-parity states in ^{63,65}Ga can be understood as the coupling of one of these configurations to positive-parity states of the respective even-even cores of the nuclei. In this picture, the $7/2^-$ states have a $[\pi\ p_{3/2} \otimes 2^+_{\rm core}]_{7/2^-}$, the $9/2^-$ states a $[\pi\ f_{5/2} \otimes 2^+_{\rm core}]_{9/2^-}$ structure. In both isotopes, the band head of the positive-parity band is formed by the $9/2^+$ state. This state results from the excitation of the unpaired proton into the $g_{9/2}$ orbital.

Results in ^{63}Ga

The TRS calculations for positive parity predict the signature $\alpha = +1/2$ to be lower in excitation energy, in agreement with the experimentally observed spins. The TRS plots for this configuration are shown in fig. 7. At $\hbar\omega = 0$ (see fig. 7a), which corresponds to a spin projection of $I_x \approx 4\hbar$, the nucleus shows a moderate deformation ($\beta_2 = 0.25$) and appears quite γ soft. The energy minimum is calculated for a triaxial shape with $\gamma = 22°$. This minimum stabilizes at higher rotational frequencies (see fig. 7b). Figure 8 shows the aligned spin I_x for this configuration in comparison with the experimental data. Also shown are the proton and neutron contributions to the spin. Whereas the proton spin increases smoothly with the rotational frequency, the gain in neutron spin —about $8\hbar$ between $\hbar\omega = 0.6$ MeV and $\hbar\omega = 1.0$ MeV— corresponds to the spin of a fully aligned $g_{9/2}$ neutron pair, indicating that the higher spin values in the positive-parity band are obtained by the alignment of two neutrons. The overall agreement between the experimental data and the calculation is good. However, the experimental values show a

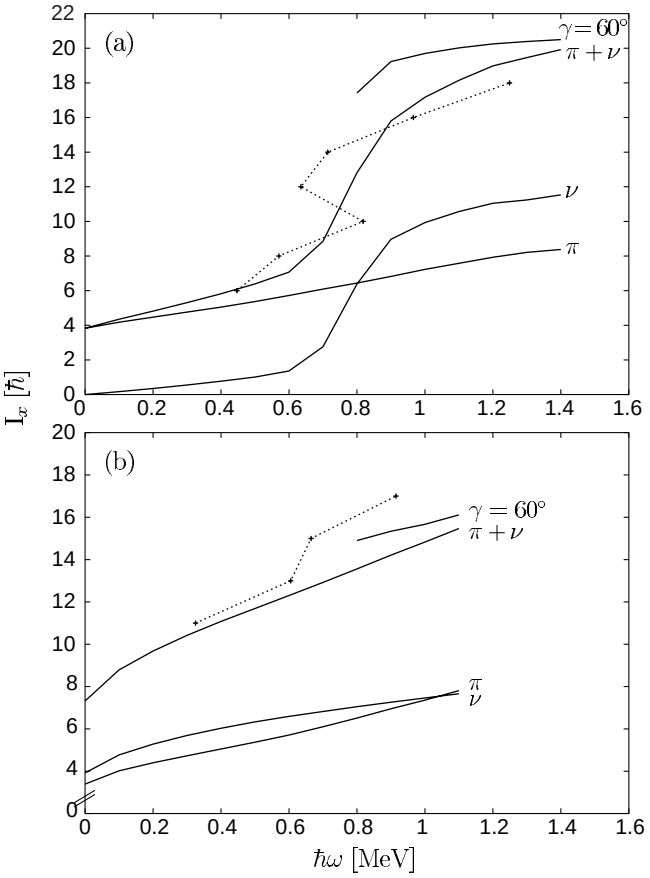

Fig. 8. Aligned spin *vs.* rotational frequency for (a) the (π, α) = (+,+1/2) and (b) the (π, α) = (–,–1/2) configurations in ^{63}Ga. The experimental values (symbols) are compared to the calculated ones (solid lines). Proton and neutron contributions are also displayed separately. For details, see text.

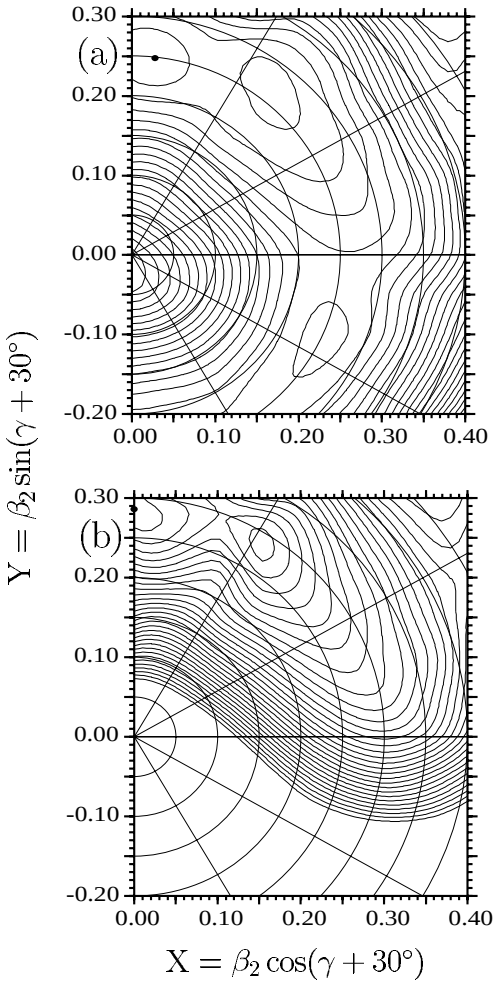

Fig. 9. Total Routhian Surfaces for positive parity in ^{65}Ga. The (+,+1/2) configuration for $\hbar\omega$ = 0.2 MeV (a) and $\hbar\omega$ = 1.2 MeV (b) are shown. The distance between the contour lines is 200 keV.

backbending between $I_x = 10\hbar$ and $I_x = 15\hbar$, which is not reproduced by the calculations. This indicates that the band interaction between the zero quasi-neutron and the two quasi-neutron configurations is weaker than predicted by the calculations.

At very high rotational frequencies, $\hbar\omega \approx 1$ MeV, the deformed collective configuration is crossed by a non-collective oblate configuration ($\beta_2 = 0.29$, $\gamma = 60°$), which terminates at $I^\pi = 41/2^+$, the maximum value for a $[\nu(g_{9/2})^2\ \nu(f_{5/2})^2\ \pi(g_{9/2})\ \pi(f_{5/2})^2\ ]$ configuration. This configuration is also included in fig. 8(a). However, due to the lack of statistics, neither the band crossing nor the terminating state have been observed in the present experiment.

The negative-parity band in ^{63}Ga is based on the $19/2^{(-)}$ state. Possible configurations for this state involve the alignment of proton and neutron pairs in the fp-shell while the unpaired proton occupies the $p_{3/2}$ orbital with negative parity and favoured signature $\alpha = -1/2$. However, in order to gain higher spin values, these configurations would require the excitation of a proton or neutron pair into the $g_{9/2}$ orbital and its alignment there. This is connected to a strong backbending, which is not observed experimentally. We therefore suggest the negative-parity states to be built on a $\pi(g_{9/2})\ \nu(g_{9/2})\ \nu(f_{5/2})$ configuration. Via Pauli blocking, the odd proton and neutron in the $g_{9/2}$ orbital prevent a backbending in the cascade built on the $19/2^-$ state. With the assumption that particle-hole excitations across the $N, Z = 28$ shell gap do not occur, the proposed configuration for the negative-parity states can be extended to $\pi(g_{9/2})\ \pi(f_{5/2})^2\ \nu(g_{9/2})\ \nu(f_{5/2})\ \nu(p_{3/2})^2$ which reaches a maximal spin of $35/2^-$ which corresponds to the 10869 keV level.

A second $35/2^-$ state at 10964 keV, a $39/2^-$ (12833 keV), and a $43/2^-$ state (14464 keV) have been identified in the experiment. Due to the exclusive decay of this cascade into the $(\pi, \alpha) = (-,-1/2)$ band similar configurations can be assumed for the states in both cascades. Based on the states in the $(\pi, \alpha) = (-,-1/2)$ cascade, the only feasible way to gain higher spins is the promotion of the $p_{3/2}$ neutron pair into the $g_{9/2}$ orbital. We therefore suggest a $\pi(g_{9/2})\ \pi(f_{5/2})^2\ \nu(g_{9/2})^3\ \nu(f_{5/2})$ configuration which can create a maximal spin of $43/2^-$.

With the spins and parity discussed in the previous chapter, the sideband reaching from spin $25/2^{(-)}$ at an excitation energy of 7914 keV up to spin $(37/2^-)$ at 12737 keV can either be interpreted as the signature partner of the negative-parity band or by the promotion of one of the $p_{3/2}$ neutrons into the $f_{5/2}$ orbital. One test for the configurations of the sideband is on the basis of the $B(M1)/B(E2)$ ratios [24,25]. The experimental values are $B(M1)/B(E2) = 2.4(3)$, 2.9(3), 1.7(1), for the 9254 keV, 10977 keV, and 12737 keV level. A possible quadrupole admixture (the mixing ratios have not been determined experimentally) in the transitions causes that these numbers overestimate the pure $B(M1)$ strength. However, the calculated values are some orders of magnitude smaller than the experimental ones, which rules out a pure $\nu(p_{3/2})$ $\alpha = +1/2$ character of the sideband. On the other hand, the calculated signature splitting for the negative-parity cascade agrees well with the experimental results. For γ deformations as obtained from the TRS calculations, the $(\pi, \alpha) = (-,+1/2)$ states are strongly mixed. The main components are the orbitals emerging from the spherical $p_{3/2}$ and the $f_{5/2}$ orbit.

Figures 7(c) and (d) show TRS plots for the $(\pi, \alpha) = (-,-1/2)$ configuration in ^{63}Ga. At rotational frequencies up to $\hbar\omega \approx 0.6$ MeV, the minimum for this configuration is predicted to lie at $\beta_2 \approx 0.28$ and $\gamma \approx 25°$ (see fig. 7(c)). The calculated spin at this frequency is $12.3\hbar$, which corresponds roughly to the $27/2^-$ state. Contrary to the positive-parity band, no backbending is observed in the $(\pi, \alpha) = (-,-1/2)$ cascade. At higher frequencies, the proton and neutron spins increase simultaneously and smoothly.

At $\hbar\omega \approx 0.9$ MeV, a configuration with $\gamma \approx 50°$ becomes yrast (see fig. 7(d)), which at even higher rotational frequencies moves towards $\gamma = 60°$. However, the corresponding states have not been observed in the experiment.

The interpretation of the negative-parity states above the $19/2^-$ level by the excitation of one neutron into the $g_{9/2}$ orbit instead of the promotion of the unpaired proton into the $f_{5/2}$ or $p_{3/2}$ orbital can also explain the striking similarity between the level schemes of ^{63}Ga and ^{64}Ge [10,26]. In ^{64}Ge, the negative-parity cascade decays via the 1665 keV $5^- \rightarrow 4^+$ transition into the ground-state band. The 5^- state is populated via the 528 keV $7^- \rightarrow 5^-$ and the 1127 keV $9^- \rightarrow 7^-$ transitions. This cascade has been extended up to spin (15^-). In ^{63}Ga, the corresponding numbers are 1772 keV $(19/2^- \rightarrow 17/2^+)$, 649 keV $(23/2^- \rightarrow 19/2^-)$, 1209 keV $(27/2^- \rightarrow 23/2^-)$, and spin $35/2^-$. The negative-parity states in ^{64}Ge are interpreted as the promotion of one particle into the $g_{9/2}$ orbital [9]. The comparison with the data now available for ^{63}Ga suggests that this particle is a neutron rather than a proton.

Results in ^{65}Ga

Figure 9(a) shows the TRS plot for the $(\pi, \alpha) = (+,+1/2)$ configuration in ^{65}Ga at a rotational frequency of $\hbar\omega \approx 0.2$ MeV. The calculated spin at this frequency corresponds to the $J^\pi = 9/2^+$ band head of the cascade. The calculated deformation parameters are $\beta_2 = 0.25$, as for the $(\pi, \alpha) = (+,+1/2)$ band in ^{63}Ga, and $\gamma = 54°$. The nucleus, however, appears to be quite γ soft: A second minimum appears at $\beta_2 = 0.25$ and $\gamma = 25°$. This deformation becomes yrast at higher rotational frequencies. The γ softness could explain the parallel structures in the positive-parity band between the $13/2^+$ and the $25/2^+$ states. The calculated deformation above the $25/2^+$ state ($\beta_2 = 0.25$, $\gamma \approx 25°$) is stable up to rotational frequency of $\hbar\omega = 1$ MeV, which corresponds to a spin of about $17\hbar$. Whereas the proton contribution to the total spin increases only slowly with the rotational frequency, additional angular momentum is gained by the alignment of a $g_{9/2}$ neutron pair (see fig. 10). Above $\hbar\omega = 1$ MeV the configuration is crossed by a non-collective one ($\beta_2 = 0.29$, $\gamma = 60°$, fig. 9(b)), which terminates at a spin of about $20.5\hbar$. The spin value is the maximal possible within a $[\nu(g_{9/2})^2\ \nu(f_{5/2})^4\ \pi(g_{9/2})\ \pi(f_{5/2})^2]$ configuration space. This terminating state is in very good agreement with the $41/2^+$ state, the highest one experimentally observed in this cascade.

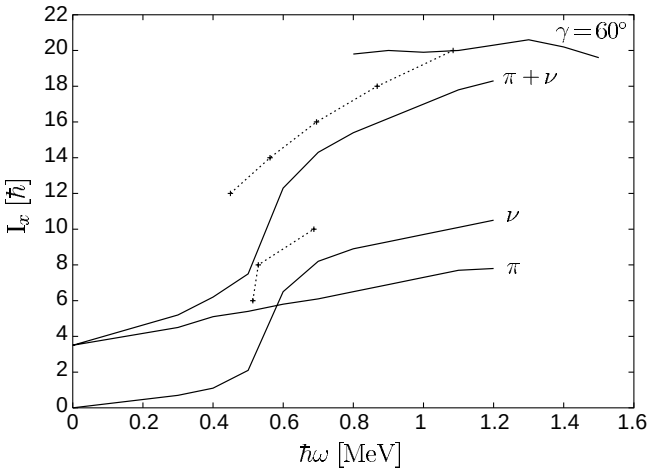

Fig. 10. Aligned spin *vs.* rotational frequency for the $(\pi, \alpha) = (+,+1/2)$ configuration in ^{65}Ga. The experimental values (symbols) are compared to the calculated ones (solid lines). Proton and neutron contributions are also displayed separately. For details, see text.

In spite of the tentative spin and parity assignments for the cascade between the $(27/2^+)$ state at $E_x = 8199$ keV and the $(43/2^+)$ state at $E_x = 15043$ keV, we will consider this sequence as the signature partner of the $(\pi, \alpha) = (+,+1/2)$ band. The $(\pi, \alpha) = (+,-1/2)$ configuration is predicted to be slightly more deformed than the $(\pi, \alpha) = (+,+1/2)$ states. For the negative signature the calculated deformation parameters are $\beta_2 = 0.29$ and $\gamma = 20°$. In contrast to the $(\pi, \alpha) = (+,+1/2)$ band, the $(\pi, \alpha) = (+,-1/2)$ configuration is not crossed by a non-collective one. The collective configuration remains yrast even at high rotational frequencies and angular momenta.

The aligned angular momentum I_x for both signatures is shown in fig. 10 in combination with the calculated values and the contributions from protons and neutrons. The alignment of the $g_{9/2}$ neutron pair at $\hbar\omega \approx 0.5$ MeV in

the $(\pi, \alpha) = (+,+1/2)$ band is clearly visible. In the experimental data as well as in the calculations the values for the aligned angular momentum I_x nearly coincide for both signatures, pointing towards similar configurations. The calculations, however, underestimate the aligned angular momentum by about $2\hbar$, whereas the slope with increasing rotational frequency is reproduced correctly.

In contrast to ^{63}Ga, negative-parity states are only weakly populated in ^{65}Ga. The probable band head of the $(\pi, \alpha) = (-,-1/2)$ cascade is the $19/2^{(-)}$ state. The calculations for the $(\pi, \alpha) = (-,-1/2)$ configuration predict a sudden gain of angular momentum at $\hbar\omega \approx 0.8$ MeV, a higher value than the experimentally observed rotational frequencies. The calculated deformation for $I_x \approx 10\hbar$, $\beta_2 = 0.33$, $\gamma = 18°$ remains stable up to high frequencies. However, due to the weak population of this band, the corresponding states could only be observed up to spin $31/2^{(-)}$ with a possible extension of the band up to $(35/2^-)$.

4 Conclusions

We have studied high-spin states in the neutron-deficient nuclei ^{63}Ga and ^{65}Ga. In both nuclei the previously known single-particle states below an excitation energy of 1.5–2.0 MeV could be confirmed. Above the $9/2^+$ states, which are formed by the promotion of the unpaired proton into the $g_{9/2}$ orbital, rotational-like structures were identified or extended in both isotopes. The level scheme of ^{63}Ga is dominated by a negative-parity sequence built on the $19/2^{(-)}$ level and reaching up to spin $43/2^{(-)}$ at an excitation energy of 14.5 MeV. These states are interpreted as being based on a $\pi(g_{9/2})\nu(g_{9/2})\nu(f_{5/2})$ configuration. The excitation of both, a proton and a neutron into the $g_{9/2}$ orbital can explain the similarity between the excitation patterns of ^{63}Ga and ^{64}Ge. The positive-parity bands in both Ga isotopes are governed by a $\nu(g_{9/2})^2$ alignment at rotational frequencies of $\hbar\omega \approx 0.7$ MeV in ^{63}Ga and $\hbar\omega \approx 0.6$ MeV in ^{65}Ga. In ^{65}Ga, the $41/2^+$ state is a likely candidate for the band termination of the $[\nu(g_{9/2})^2\ \nu(f_{5/2})^4\ \pi(g_{9/2})\ \pi(f_{5/2})^2]$ configuration.

The authors would like to thank the operational staff of the Tandem XTU accelerator of LNL for their assistance during the experiment. The work was supported by the Swedish Natural Science Research Council.

References

1. D. Rudolph, C. Baktash, M.J. Brinkman, M. Devlin, H.-Q. Jin, D.R. LaFosse, L.L. Riedinger, D.G. Sarantites, C.-H. Yu, Eur. Phys. J. A **4**, 115 (1999).
2. G. de Angelis, C. Fahlander, A. Gadea, E. Farnea, W. Gelletly, A. Aprahamian, D. Bazzacco, F. Becker, P.G. Bizzeti, A. Bizzeti-Sona, F. Brandolini, D. de Acuna, M. De Poli, J. Eberth, D. Foltescu, S.M. Lenzi, S. Lunardi, T. Martinez, D.R. Napoli, P. Pavan, C.M. Petrache, C. Rossi Alvarez, D. Rudolph, B. Rubio, W. Satula, S. Skoda, P. Spolaore, H.G. Thomas, C.A. Ur, R. Wyss, Phys. Lett. B **415**, 217 (1997).
3. C.J. Lister, P.J. Ennis, A.A. Chishti, B.J. Varley, W. Gelletly, H.G. Price, A.N. James, Phys. Rev. C **42**, R1191 (1990).
4. D.P. Balamuth, U.J. Hüttmeier, T. Chapuran, D.G. Popescu, J.W. Arrison, Phys. Rev. C **43**, 2082 (1991).
5. I. Dankó, D. Sohler, Zs. Dombrádi, S. Brant, V. Kristić, J. Cederkäll, M. Lipoglavšek, M. Palacz, J. Persson, A. Atac, C. Fahlander, H. Grawe, A. Johnson, A. Kerek, W. Klamra, J. Kownacki, A. Likar, L.-O. Norlin, J. Nyberg, V. Paar, R. Schubart, D. Seweryniak, D. Vretenar, G. de Angelis, P. Bednaczyk, D. Foltescu, D. Jerrestam, S. Juutinen, E. Mäkelä, B. M. Nyakó, M. de Poli, H.A. Roth, T. Shizuma, Ö. Skeppstedt, G. Sletten, S. Törmänen, Phys. Rev. C **59**, 1956 (1999).
6. T. Steinhardt, Diploma thesis, University of Cologne, unpublished.
7. S.M. Vincent, P.H. Regan, D. Blumenthal, M. Carpenter, C.N. Davids, W.Gelletly, R.V.F. Janssens, C.J. Lister, D. Seweryniak, J. Schwartz, J. Simpson, D.D. Warner, J. Phys. G **25**, 679 (1999).
8. A. Juodagalvis, S. Åberg, Nucl. Phys. A **683**, 207 (2001).
9. G. de Angelis, C. Fahlander, A. Gadea, E. Farnea, W. Gelletly, A. Aprahamian, A. Axelsson, D. Bazzacco, F. Becker, P.G. Bizzeti, A. Bizzeti-Sona, F. Brandolini, D. de Acu na, M. De Poli, J. Eberth, D. Foltescu, S. Lenzi, S. Lunardi, T. Martinez, D.R. Napoli, P. Pavan, C.M. Petrache, C. Rossi Alvarez, D. Rudolph, B. Rubio, S. Skoda, P. Spolaore, G. Thomas, C. Ur, M. Weiszflog, R. Wyss, Nucl. Phys. A **630**, 426c (1998).
10. E. Farnea, A. Gadea, G. de Angelis, J. Eberth, T. Steinhardt, O. Thelen, A. Algora, D. Bazzacco, N. Belcari, P.G. Bizzeti, A.M. Bizzeti-Sona, F. Brandolini, M. De Poli,A. Dewald, C. Fahlander, E. Fioretto, W. Gelletly, R. Isocrate, N. Kintz, S.M. Lenzi, S. Lunardi, T. Martinez, D.R. Napoli, J. Nyberg, P. Pavan, C.M. Petrache, G.F. Prete, C. Rossi Alvarez, B. Rubio, D. Rudolph, S. Skoda, P. Spolaore, J.L. Tain, M. Weiszflog, R. Wyss, in *Proceedings "Pingst 2000 - Selected Topics on N = Z nuclei", Lund, Sweden, June 2000*, edited by D. Rudolph, M. Hellström, (KFS AB Lund, 2000).
11. D. Bazzacco, *Proceedings of the International Conference on Nuclear Structure at High Angular Momentum, Ottawa, 1992*, Report No. AECL 10613, Vol. II (AECL Research, Ottawa, 1992) p. 376.
12. E. Farnea, G. de Angelis, M. De Poli, D. De Acuna, A. Gadea, D.R. Napoli, P. Spalaore, A. Buscemi, R. Zanon, R. Isocrate, D. Bazzacco, C. Rossi Alvarez, P. Pavan, A.M. Bizzeti-Sona, P.G. Bizzeti, Nucl. Instrum. Methods A **400**, 87 (1997).
13. K.S. Krane, R.M. Steffen, R.M. Wheeler, Nucl. Data Tables **11**, 351 (1973).
14. M. Piiparinen, A. Ataç, J. Blomqvist, G.B. Hagemann, B. Herskind, R. Julin, S. Juutinen, A. Lampinen, J. Nyberg, G. Sletten, P. Tikkanen, A. Vertanen, R. Wyss, Nucl. Phys. A **605**, 191 (1996).
15. R.M. Diamond, E. Matthias, J.O. Newton, F.S. Stephens, Phys. Rev. Lett. **16**, 1205 (1966).
16. G.H. Dulfer, H.E. Beertema, H. Verheul, Nucl. Phys. A **149**, 518 (1970).

17. H.W. Jongsma, J.C. de Lange, H. Verheul, FW.N. de Beur, P.F.A. Goudsmit, Z. Phys. **262**, 247 (1973).
18. M.G. Betigeri, H.H. Duhm, R. Santo, R. Stock, R. Bock, Nucl. Phys. A **100**, 416 (1967).
19. R.G. Couch, J.A. Biggerstaff, F.G. Perey, S. Raman, K.K. Seth, Phys. Rev. C **2**, 149 (1970).
20. N. Belcari, G. de Angelis, J. Eberth, S. Skoda, R. Wyss, E. Farnea, A. Gadea, A. Algora, M. De Poli, E. Fioretto, T. Martínez, D.R. Napoli, G. Prete, P. Spolaore, D. Bazzacco, F. Brandolini, A. Buscemi, R. Isocrate, S. Lenzi, S. Lunardi, R. Menegazzo, C.M. Petrache, P. Pavan, C. Rossi-Alvarez, Zs. Podolyák, P.G. Bizzeti, A.M. Bizzeti-Sona, LNL-INFN Rep. 139/99 (1999).
21. H. Kawakami, A.P. de Lima, R.M. Ronningen, A.V. Ramayya, J.H. Hamilton, R.L. Robinson, H. J. Kim, L.K. Peker, Phys. Rev. C **21**, 1311 (1980).
22. W. Satula, R. Wyss, Phys. Scr. T **56**, 159 (1995).
23. W. Satula, R. Wyss, Phys. Lett. B **393**, 1 (1997).
24. F. Dönau, S. Frauendorf, in *Proceedings of the Conference on High Angular Momentum Properties in Nuclei, Oak Ridge, 1982*, edited by N.R. Johnson (Harwood Academic, New York, 1983), p. 143.
25. F. Dönau, Nucl. Phys. A **471**, 469 (1987).
26. P.J. Ennis, C.J. Lister, W. Gelletly, H.G. Price, B.Varley, P.A. Butler, T. Hoare, S. Cwiok, W. Nazarewicz, Nucl. Phys. A **535**, 392 (1991).